Effect of high temperature neutron irradiation on fracture toughness of ITER-specification tungsten

C. Yin[a,b,], D. Terentyev[a], S. Van Dyck[a], A. Stankovskiy[a], R. H. Petrov[c,d] and T. Pardoen[b]*

[a]Structural Materials Group, Institute of Nuclear Materials Science, SCK-CEN, 2400 Mol, Belgium; [b]Institute of Mechanics, Materials and Civil Engineering, UCLouvain, 1348 Louvain-la Neuve, Belgium; [c]*Department of Electrical Energy, Metals, Mechanical Constructions & Systems, Ghent University, 9052 Ghent, Belgium;* [d] *Department of Materials Science and Engineering , Delft University of Technology, Delft , 2082, The Netherlands*

First e-mail: cyin@sckcen.be

The effect of neutron irradiation on the fracture toughness of two commercially pure tungsten materials processed according to ITER specification has been investigated for three doses 0.08 dpa, 0.44 dpa, and 0.67 dpa at 600 °C. The choice of this temperature was motivated by its technological importance due to the risk of irradiation-induced embrittlement. The temperature of 600 °C is below the void swelling peak temperature (~800 °C) and, at the same time, well above the ductile to brittle transition temperature (DBTT) of the reference material (~300 °C). Neutron irradiation was performed in the BR2 material test reactor inside the fuel channel in order to limit the transmutation of rhenium and osmium close to the rates expected in fusion environment. The results of the mechanical tests performed up to 600 °C show that the fracture toughness decreases with increasing the irradiation dose for both tungsten products. The fracture surfaces of the non- and irradiated specimens were systematically analysed to determine the evolution of the failure mechanisms.

*Corresponding author: tel.: +32-33-31-86 , e-mail: cyin@sckcen.be (C. Yin)

Introduction

Neutron irradiation effect on mechanical properties of tungsten is considered to be a key element in the design of the plasma facing components (PFC) for ITER at the nuclear phase operation [1-3]. The divertor PFC will be exposed to high heat flux load during normal operation where the temperature from the contact with the heat sink material to the top surface varies from 300 °C to 1200 °C (for power load of 15 MW/m^2) [4]. Therefore, a database of mechanical properties accounting for the combination of the temperature gradient and neutron irradiation is required.

Currently, tungsten is the main candidate material for plasma facing components including the divertor of ITER and the first wall armor in DEMO, where much higher neutron flux compared to ITER is expected. Up to now, most of the studies on the neutron irradiation effects on mechanical properties of tungsten were focused on modeling and measurement of hardness [5-14]. However, the latter was performed at room temperature, which cannot be considered as a representative test condition for PFCs. Only few studies, performed in the 1970s and after 2016, addressed the change of tensile and bending properties of tungsten, which was irradiated by neutrons in fast and mixed spectra reactors including high temperature irradiation and testing, namely up to 800 ^{o}C [15-17]. Up to now, no information on the change of the fracture toughness after neutron irradiation is available, while this gap needs to be closed to perform at least a computational assessment of the structural integrity of PFCs in normal and off-normal operating regimes [18].

The aim of this study is to investigate the change of fracture toughness and fracture surface morphology after neutron irradiation at 0.08, 0.44, and 0.67 dpa of two tungsten products fabricated according to the ITER specification [19]. The selected doses for neutron irradiation refer to the accumulated end-of-life dose in ITER PFC, which is expected to be less than 1 dpa [20]. The irradiation and maximum test temperature has been selected at 600 ^{o}C, below the peak swelling [21-23], and yet considerably above the ductile to brittle transition temperature (DBTT) of typical commercial tungsten products [24, 25].

Methodology

Two ITER specification tungsten products are considered in this study: IGP (manufactured by Plansee, Austria by double hammering and supplied as rod) and CFETR (manufactured by AT&M, China by rolling and supplied in a shape of plate). As a result, IGP has elongated carrot-like grains aligned in the longitudinal direction (LD) whereas CFETR has flat pancake-like grains “flattened” along the rolling direction (RD) [26]. The equivalent median diameter of a grain (defined by a high angle grain boundary with a misorientation angle between grains larger than 15^{o}), measured on the plane perpendicular to the normal direction (ND), is around 100 µm and 70 µm for IGP and CFETR, respectively. Additionally, a sub-grain structure (misorientation angle between 5 to 15^{o}) with a sub-grain size of several µm was observed in both materials. More detailed information on the microstructure and mechanical properties of these products can be found in our previous work [26].

Disk-shaped compact tension (DCT) specimens were machined with a narrow notch having a root radius around 50-90 µm produced by EDM. The notch machined in the specimens for both materials is parallel to the T-L plane, as imposed in the ASTM E399 standard [27]. A schematic of the specimen geometry with dimensions is shown in Figure 1a.

Neutron irradiation was performed in the Belgian Material Test Reactor (BR2) inside the fuel element in the position close to the center of the reactor and in a mid-plane where the fast neutron (E > 0.1 MeV) flux is 7×10^{14} n/cm^2/s at a power of 60 MW. The samples were encapsulated in a steel tube with 1.5 mm wall thickness filled with He. The gap between the samples and the pressure tube was adjusted to achieve 600 ^{o}C during the irradiation following the thermal and neutronic calculations. Following finite element analysis of thermal flow, a variation of about 25 ^{o}C could occur due to the burn out of the fuel element within a reactor cycle. The irradiation dose was calculated by MCNPX 2.7.0 [28] and found to be 0.08 dpa, 0.44 dpa, and 0.67 dpa. The dpa cross sections for W have been estimated from the JENDL4 file (MT444) for the threshold displacement energy of 55 eV, following the recommendation of IAEA [29]. The transmutation of Re and Os is calculated based on the ALEPH code developed by SCK•CEN and available nuclear databases [30-34]. The upper limit of the summed concentration (at%) of Re and Os together is 0.61 at%, 0.97 at%, and 1.40 at% for 0.08 dpa, 0.44 dpa, and 0.67 dpa, respectively. The fraction of Os is about 1 % of the totally produced Re and Os.

K_{Jc} values (elastic-plastic equivalent stress intensity factor) of the irradiated specimens are determined according the requirements of the ASTM E1921 [35]. The fracture toughness tests for irradiated and non-irradiated specimens are carried out in air using an universal testing machine (INSTRON 3800) with an environmental furnace. The test temperature for irradiated specimens ranges from 400 °C to 580 °C. In order to get homogenous temperature distribution and to limit surface oxidation, the heated specimens are exposed to an elevated temperature for only 30 minutes prior to the start of the test. The test itself lasted for a few minutes or less. The reference measurements were reported in our previous work [26]. The qualitative and quantitative analyses of the microstructures of the fracture surfaces (fraction of fracture type) were carried out by ImageJ analysis software on scanning electron microscopy (SEM) images at appropriate magnifications.

In this paper, we present the results of mechanical tests performed for both products at 0.08 dpa, and higher dose data are shown for CFETR tungsten only. Our preliminary study had shown that the fracture toughness of the IGP irradiated to 0.44 dpa requires testing to be performed above 600 °C, which is the upper limit of this study.

Results and discussion

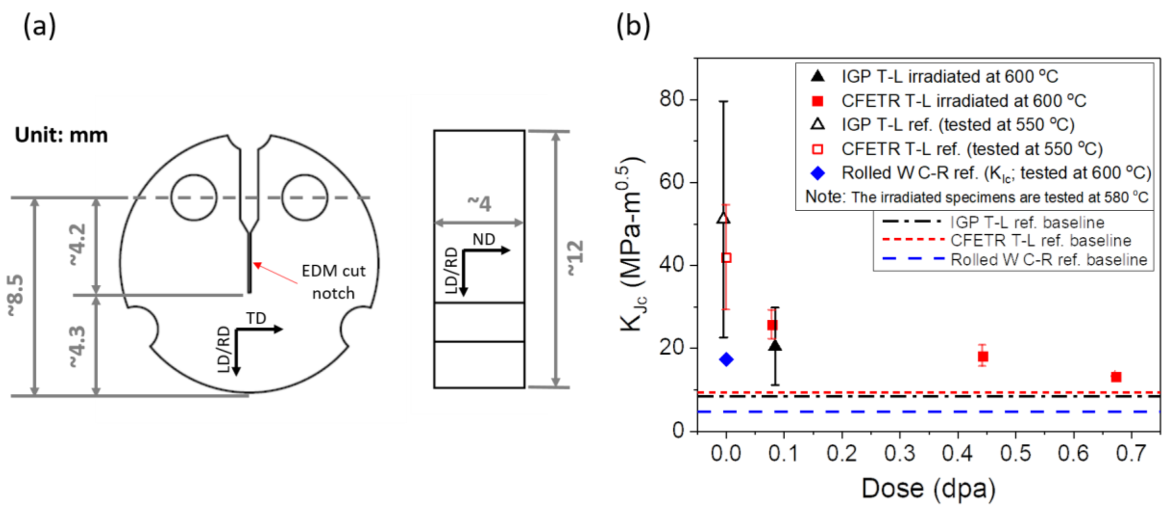

Figure 1. (a) Sketch and dimensions of DCT specimens (TD: transverse direction; ND: normal direction); (b) K_{Jc} as a function of irradiation dose for IGP T-L and CFETR T-L (the data of reference specimens is referred to our previous work [26]; the K_{Ic} value (only considers linear elastic fracture behavior) of Rolled W C-R, which can be considered as the lower limit of the fracture toughness, is referred to Faleschini, et al [36]); the baselines are defined as the fracture toughness at room temperature; more than two specimens were tested at each test temperatures to obtain minimum statistics; the error bars represent one standard deviation of the experimental data

Figure 1b shows the variation of the fracture toughness with irradiation dose, together with the reference values measured at room temperature i.e. in the brittle, non-irradiated conditions. For both tested products, the measured K_{Jc} value decreases with increasing irradiation dose. At the highest dose studied here (0.67 dpa), the K_{Jc} value of CFETR T-L is reduced almost down to the fracture toughness at room temperature. This indicates that the irradiation to 0.67 dpa has raised the DBTT of this product up to ~600 °C, which corresponds to an increase of 300 °C (see Ref. [26] for reference measurements). The irradiation-induced changes of microstructure in the studied samples is currently under investigation. However, as reported in the literature [12], the hardening and subsequent embrittlement induced by neutron irradiation depend not only on the fluence and irradiation temperature but also on the neutron spectrum, which defines the transmutation rate. Transmuted elements (Re and Os) are found to form secondary phases (σ phase and χ phase), while displacement damage creates voids and dislocation loops in the temperature and dose range studied here [11, 13]. The presence of precipitates, voids and dislocation loops decreases the mobility of dislocations causing hardening. As a result, the ductility and capacity to dissipate energy by plastic deformation of irradiated material is reduced such that it loses its fracture toughness i.e. becomes brittle. Moreover, the irradiation-induced defects can also act as stress concentration sites thus affecting the crack propagation not only below and but also above the DBTT region.

The amount by which K_{Jc} is reduced by the irradiation is different for the two types of tested materials. IGP T-L exhibits a larger reduction of K_{Jc} compared to the CFETR T-L product. In addition, the scatter in the K_{Jc} value also decreases with increasing the irradiation dose. This is probably related to the fact the neutron irradiation induced defects, homogeneously distributed in the material, also act as stress concentrators reducing the statistical spread of the defects controlling the fracture of the non-irradiated state.

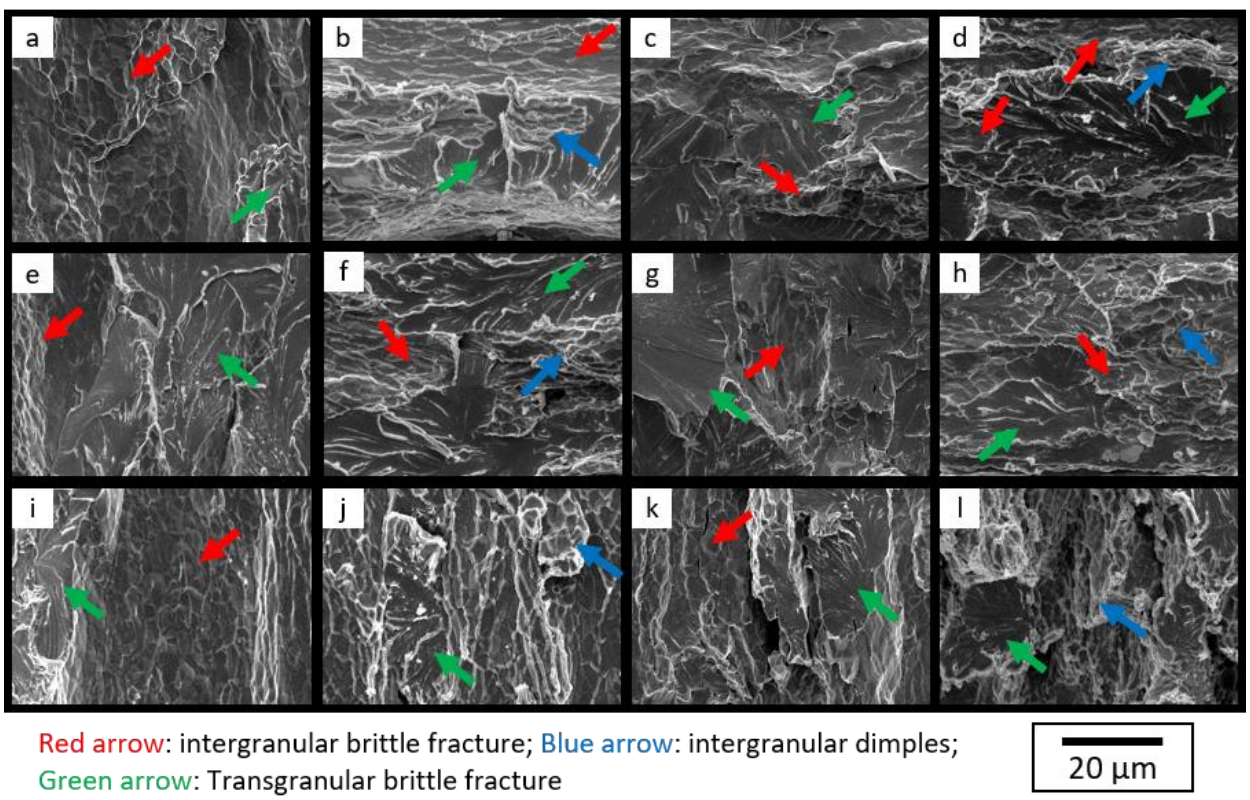

Red arrow: intergranular brittle fracture; Blue arrow: intergranular dimples; Green arrow: Transgranular brittle fracture

Figure 2. Fracture surfaces of the DCT specimens. IGP T-L 0.08 dpa tested at 500 °C (a) and 580 °C (b); CFETR T-L 0.08 dpa tested at 400 °C (c) and 580 °C (d); CFETR T-L 0.44 dpa tested at 500 °C (e) and 580 °C (f); CFETR T-L 0.67 dpa tested at 500 °C (g) and 580 °C (h); IGP T-L reference tested at 500 °C (i) and 600 °C (j); CFETR T-L reference tested at 500 °C (k) and 600 °C (l)

Figure 2 shows a collection of the fracture surface morphologies from which transgranular surface fraction has been determined. The morphology of the fracture patterns of both materials, although tested after different irradiation doses, look quite similar. At temperature below 550 °C (Figure 2a, c, e, g, i, k), the fracture surface of all specimens, no matter if they were irradiated or not, exhibit a mixture of intergranular and transgranular brittle fracture. However, intergranular ductile dimples start to appear at the test temperature above 550 °C (Figure 2b, d, f, h, j, l) for non-irradiated and irradiated specimens. When the test temperature rises up to 600 °C, the intergranular brittle fracture is no longer observed in the non-irradiated materials, as reported in [26] as well. The fact that the intergranular brittle fracture mode disappears on the fracture surface of irradiated specimens at test temperature equal to 600 °C will require further investigation.

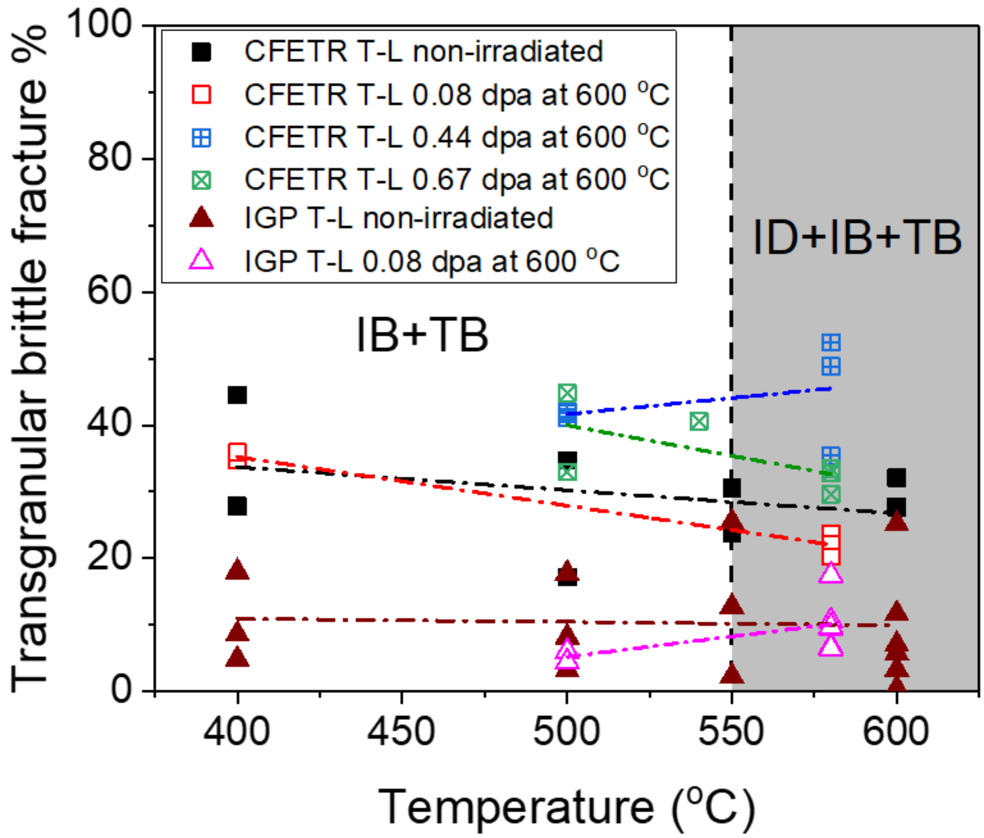

Figure 3. Variation of the fraction of transgranular brittle fracture as a function of test temperature: each data point in the plot represents the fraction of fracture feature corresponding to one specimen. IB: Intergranular Brittle; TB: Transgranular Brittle; ID: Intergranular Dimple

The surface ratio of transgranular brittle fracture mode, as calculated by ImageJ analysis of the SEM images, is given in Figure 3. For most of the inspected conditions, the fraction of transgranular brittle fracture is larger in the CFETR product. Moreover, for the CFETR product, the fraction of transgranular brittle fracture is seen to increase with increasing the irradiation dose, which is likely related to the suppression of dislocation-mediated plasticity inside the grains caused by the presence of the irradiation-induced defects (dislocation loops, voids and probably Re/Os precipitates). In the case of the IGP T-L product, the irradiation at 0.08 dpa does not impact the amount of transgranular brittle fracture. This difference between the fracture patterns of the IGP and CFETR materials can be ascribed to the difference in the shape of grains, and mutual grain-crack orientation in the studied products [26]. IGP has carrot-like grains along the crack propagation direction and CFETR has pancake-like grains perpendicular to the crack propagation plane [26]. As a result, the IGP exhibits a lower propensity for transgranular brittle fracture than the CFETR product [26]. The confirmation of this hypothesis, as well as a physical explanation for the observed embrittlement, requires detailed transmission electron microscopy study as well as the measurement of the chemical composition (i.e. Re and Os) in the irradiated samples, which is currently in progress.

Conclusions

Based on the results obtained up to now, we can draw the following conclusions:

(i) K_{Jc} measured at 580 ^{o}C progressively decreases with increasing irradiation dose down to ~ 10 $\mathrm{MPa}\cdot\sqrt{m}$ i.e. approaching the room temperature fracture toughness of this material. This indicates that neutron irradiation at 600 ^{o}C, which is similar to the condition to be faced by divertor tungsten monoblock in the region close to the cooling pipe, leads to the shift of DBTT by 300 ^{o}C as the neutron fluence progressively increases i.e. the irradiation makes the material brittle under the irradiation condition. Note that the dose of 0.67 dpa is close to the design end-of-life dose for the ITER divertor components. However, the concentration of transmuted elements after irradiated in BR2 is different (approximately factor of two higher) from the one expected in fusion environment due to a higher fraction of thermal-to-fast neutrons. Understanding of the impact of enhanced transmutation due to fission environment remains a truly challenging problem for which the most natural solution is the application of fast fission spectrum (i.e. usage of CEFR or BOR60 reactors).

(ii) The appearance of dimples on the fracture surface (at T_{test} > 550 ^{o}C) seems to be the only clear temperature dependent microstructural feature observed by SEM in this study.

(iii) The portion of transgranular brittle fracture pattern in the CFETR T-L material increases after irradiation, which can be explained by the obstruction of plastic deformation of grains due to pinning of dislocations at irradiation-induced defects. However, the same trend is not observed in the IGP T-L material.

Acknowledgement

This work has been carried out within the framework of the EUROfusion Consortium and has received funding from the Euratom research and training programme 2014–2018 and 2019-2020 under grant agreement No 633053. The views and opinions expressed herein do not necessarily reflect those of the European Commission.

Reference

[1] Davis J, Barabash V, Makhankov A, Plöchl L, Slattery K. Assessment of tungsten for use in the ITER plasma facing components. J Nucl Mater. 1998;258:308-312.

[2] Zinkle S, Ghoniem N. Operating temperature windows for fusion reactor structural materials. Fusion Eng Des. 2000;51:55-71.

[3] Barabash V, Federici G, Rödig M, Snead L, Wu C. Neutron irradiation effects on plasma facing materials. J Nucl Mater. 2000;283:138-146.

[4] You J, Visca E, Barrett T, Böswirth B, Crescenzi F, Domptail F, et al. European divertor target concepts for DEMO: Design rationales and high heat flux performance. Nuclear Materials and Energy. 2018;16:1-11.

[5] Huang C-H, Gilbert MR, Marian J. Simulating irradiation hardening in tungsten under fast neutron irradiation including Re production by transmutation. J Nucl Mater. 2018;499:204-215.

[6] Zhao Q, Zhang Z, Huang M, Ouyang X. Effects of transmutation elements in tungsten. Computational Materials Science. 2019;162:133-139.

[7] Hu X, Koyanagi T, Fukuda M, Kumar NK, Snead LL, Wirth BD, et al. Irradiation hardening of pure tungsten exposed to neutron irradiation. J Nucl Mater. 2016;480:235-243.

[8] Hasegawa A, Tanno T, Nogami S, Satou M. Property change mechanism in tungsten under neutron irradiation in various reactors. J Nucl Mater. 2011;417(1-3):491-494.

[9] Hasegawa A, Fukuda M, Tanno T, Nogami S. Neutron irradiation behavior of tungsten. Materials transactions. 2013:MG201208.

[10] Fukuda M, Hasegawa A, Tanno T, Nogami S, Kurishita H. Property change of advanced tungsten alloys due to neutron irradiation. J Nucl Mater. 2013;442(1-3):S273-S276.

[11] Hasegawa A, Fukuda M, Nogami S, Yabuuchi K. Neutron irradiation effects on tungsten materials. Fusion Eng Des. 2014;89(7-8):1568-1572.

[12] Fukuda M, Kumar NK, Koyanagi T, Garrison LM, Snead LL, Katoh Y, et al. Neutron energy spectrum influence on irradiation hardening and microstructural development of tungsten. J Nucl Mater. 2016;479:249-254.

[13] Hasegawa A, Fukuda M, Yabuuchi K, Nogami S. Neutron irradiation effects on the microstructural development of tungsten and tungsten alloys. J Nucl Mater. 2016;471:175-183.

[14] Katoh Y, Snead L, Garrison L, Hu X, Koyanagi T, Parish C, et al. Response of unalloyed tungsten to mixed spectrum neutrons. J Nucl Mater. 2019;520:193-207.

[15] Garrison L, Katoh Y, Snead LL, Byun TS, Reiser J, Rieth M. Irradiation effects in tungsten-copper laminate composite. J Nucl Mater. 2016;481:134-146.

[16] Garrison LM, Katoh Y, Kiran Kumar NAP. Mechanical properties of single-crystal tungsten irradiated in a mixed spectrum fission reactor. J Nucl Mater. 2019;518:208-225.

[17] Habainy J, Dai Y, Lee Y, Iyengar S. Mechanical properties of tungsten irradiated with high-energy protons and spallation neutrons. J Nucl Mater. 2019;514:189-195.

[18] Li MY, You JH. Interpretation of the deep cracking phenomenon of tungsten monoblock targets observed in high-heat-flux fatigue tests at 20 MW/m^2. Fusion Eng Des. 2015;101:1-8.

[19] Hirai T, Panayotis S, Barabash V, Amzallag C, Escourbiac F, Durocher A, et al. Use of tungsten material for the ITER divertor. Nuclear Materials and Energy. 2016;9:616-622.
[20] Villari R, Barabash V, Escourbiac F, Ferrand L, Hirai T, Komarov V, et al. Nuclear analysis of the ITER full-tungsten divertor. Fusion Eng Des. 2013;88(9-10):2006-2010.
[21] Matolich J, Nahm H, Moteff J. Swelling in neutron irradiated tungsten and tungsten-25 rhenium. Scripta Metallurgica. 1974;8:837-842.
[22] Stork D, Agostini P, Boutard JL, Buckthorpe D, Diegele E, Dudarev S, et al. Developing structural, high-heat flux and plasma facing materials for a near-term DEMO fusion power plant: the EU assessment. J Nucl Mater. 2014;455(1-3):277-291.
[23] Lee F, Matolich J, Moteff J. Swelling in neutron irradiated molybdenum based on dimensional changes. J Nucl Mater. 1976;62(1):115-117.
[24] Gludovatz B, Wurster S, Hoffmann A, Pippan R. Fracture toughness of polycrystalline tungsten alloys. International Journal of Refractory Metals & Hard Materials. 2010;28(6):674-678.
[25] Wurster S, Baluc N, Battabyal M, Crosby T, Du J, Garcia-Rosales C, et al. Recent progress in R&D on tungsten alloys for divertor structural and plasma facing materials. J Nucl Mater. 2013;442(1-3):S181-S189.
[26] Yin C, Terentyev D, Pardoen T, Petrov R, Tong Z. Ductile to brittle transition in ITER specification tungsten assessed by combined fracture toughness and bending tests analysis. Materials Science & Engineering: A. 2019;750:20-30.
[27] ASTM. E 399-12. Standard test method for linear-elastic plane strain fracture toughness KIC of metallic materials. West Conshohocken, PA. ASTM international. 2012
[28] Pelowitz D, Durkee J, Elson J, Fensin M, James M, Johns R, et al. MCNPX 2.7. 0 Extensions. LA-UR-11-02295 ed: Los Alamos National Laboratory; 2011.
[29] Dudarev SL. DPA definition and estimates: IAEA CRP; 2015. Available from: https://www-amdis.iaea.org/CRP/IrradiatedTungsten/RCM2/RCM2Presentation-DudarevDPA-2015-09-10.pdf.
[30] Stankovskiy A, Van den Eynde G, Fiorito L. ALEPH V.2.7, A Monte Carlo Burn-Up Code. ALEPH V.2.7 ed: SCK•CEN; 2018.
[31] JEFF-3.3 [Internet]. Nuclear Energry Agency. 2017. Available from: https://www.oecd-nea.org/dbdata/jeff/jeff33/.
[32] Brown DA, Chadwick M, Capote R, Kahler A, Trkov A, Herman M, et al. ENDF/B-VIII. 0: the 8th major release of the nuclear reaction data library with CIELO-project cross sections, new standards and thermal scattering data. Nuclear Data Sheets. 2018;148:1-142.
[33] Konobeyev AY, Fischer U, Korovin YA, Simakov S. Evaluation of effective threshold displacement energies and other data required for the calculation of advanced atomic displacement cross-sections. Nuclear Energy and Technology. 2017;3(3):169-175.
[34] Norgett M, Robinson M, Torrens I. A proposed method of calculating displacement dose rates. Nuclear engineering and design. 1975;33(1):50-54.
[35] ASTM. E1921-16. Standard test method for determination of reference temperature, T0, for ferritic steels in the transition range. West Conshohocken, PA. ASTM international. 2016
[36] Faleschini M, Kreuzer H, Kiener D, Pippan R. Fracture toughness investigations of tungsten alloys and SPD tungsten alloys. J Nucl Mater. 2007;367:800-805.